A Zero-Order-Closure Turbulent Flux-Conservation Technique for Blending Refractivity Profiles in the Marine Atmospheric Boundary Layer

Robert E. Marshall[1], Victor R. Wiss[2], Katherine L. Horgan[2], William D. Thornton[2], and Janet K. Stapleton[2]

[1]Mount Pleasant Meteorology
Woodford, Virginia, USA
Tel: +1 (804) 867-7203
E-mail: mpmet@sprynet.com

[2]Naval Surface Warfare Center
Dahlgren Division
Dahlgren, Virginia, USA

Abstract

Recent advances in mesoscale numerical weather prediction (NWP) models have supported four-dimensional (4D) radio-frequency (RF) propagation modeling in challenging heterogeneous refractive marine environments. Numerical weather prediction models typically provide a vertical profile of refractivity every 1 km to 3 km horizontally in the domain of interest for each hour in a 48-hour forecast. Due to surface roughness and turbulence constraints, these profiles extend from the stratosphere to within 5 m to 10 m of the sea's surface. Because of strong evaporation at the sea's surface, significant impacts on RF system performance can be induced by refractivity gradients in the first 10 m above sea level (ASL). Historically, the lower-layer refractivity profiles have been calculated using Monin-Obukhov-Similarity- (MOS) based turbulence models. This dual-model approach requires a robust technique for blending on the order of 10^3 profiles per forecast hour without creating non-physical refractivity artifacts. This paper describes a zero-order-closure turbulent-flux technique for blending numerical weather prediction and Monin-Obukhov Similarity refractivity profiles, and presents the results of a multi-wavelength data-comparison process.

1. Introduction

Refraction of RF energy in the atmosphere is determined by the vertical structure of refractivity (N). Atmospheric pressure, atmospheric temperature, and partial pressure due to water vapor contribute to N [1, 2]. This relationship is given by

$$N = (n-1)10^6 \tag{1}$$

$$= \frac{77.6}{T}\left(p + \frac{4810e}{T}\right),$$

where n is the refractive index, T [K] is the atmospheric temperature, p [hPa] is the total atmospheric pressure, and e [hPa] is the partial pressure due to water vapor. $N(z)$ is the vertical profile of N for height z above the surface of the Earth.

The modified refractivity, M, removes the effects of the Earth's curvature from propagation calculations, allowing the use of Cartesian instead of cylindrical coordinates [3]. The vertical profile of M as a function of the height above the Earth's surface is given by

$$M(z) = N(z) + \frac{10^6 z}{a} \tag{2}$$

$$= N(z) + 0.157z,$$

where z [m] is the height above the surface, and a [m] is the mean radius of the Earth (6.378×10^6 m). The vertical gradient of $M(z)$ determines the refractive regime of the marine atmospheric boundary layer (MABL).

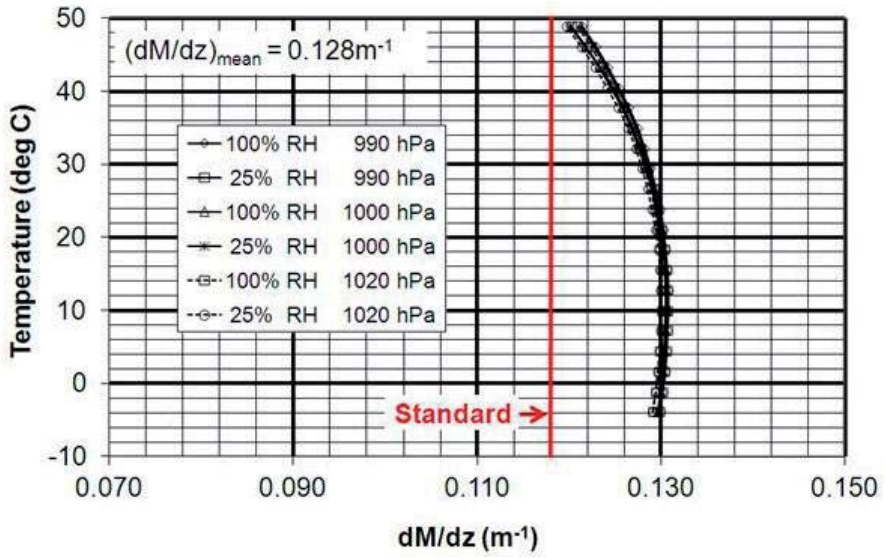

Figure 1. The vertical gradient of modified refractivity in a well-mixed marine atmospheric boundary layer.

The vertical thermodynamic structure of the marine atmospheric boundary layer is traditionally described in terms of potential temperature (θ) and water-vapor mixing ratio (w), since these are conserved variables of an air parcel if it experiences only adiabatic transformation with no net heat transfer as it moves in turbulent eddies throughout the marine atmospheric boundary layer [4]. The blending technique described in this paper is unique, since it is performed on θ , w, and p. The potential temperature in terms of T in Equation (1) is given by

$$\theta = T\left(\frac{p_0}{p}\right)^{\frac{R}{c_p}} . \qquad (3)$$

The reference pressure, p_0, is 1000 hPa. The gas constant for dry air, R, has the value 2.87×10^2 $\mathrm{Jkg^{-1}K^{-1}}$ The specific heat of dry air at constant pressure, c_p, is 1.00467×10^3 $\mathrm{Jkg^{-1}K^{-1}}$.

The water-vapor mixing ratio (w) is given by

$$w = \frac{0.622e}{p-e} \approx \frac{0.622e}{p} . \qquad (4)$$

Inserting Equations (1), (3), and (4) into Equation (2) yields

$$M = \left[\frac{77.6}{\grave{e}\left(\frac{p}{1000}\right)^{0.286}}\right]\left[P + \frac{4810\frac{wp}{0.622}}{\theta\left(\frac{p}{1000}\right)^{0.286}}\right] + 0.157z \qquad (5)$$

The vertical gradient of Equation (5) is given by

$$\frac{dM}{dz} = \frac{dp}{dz}\left(\frac{1.336\times10^7 w}{\theta^2 p^{0.572}} + \frac{399.54}{\theta p^{0.286}}\right)$$

$$-\frac{d\theta}{dz}\left(\frac{6.212\times10^7 wp^{0.428}}{\theta^3} + \frac{559.6p^{0.714}}{\theta^2}\right)$$

$$+0.157\ \mathrm{m^{-1}} . \qquad (6)$$

The marine atmospheric boundary layer is often well mixed, due to mechanical and convective turbulence [5]. In a well-mixed layer, θ and w are conserved, and thus

$$\frac{d\theta}{dz} = \frac{dw}{dz} = 0 .$$

The vertical gradient of M for a well-mixed layer is reduced to

$$\frac{dM}{dz} = \frac{dp}{dz}\left(\frac{1.336\times10^7 w}{\theta^2 p^{0.572}} + \frac{3.995\times10^2}{\theta p^{0.286}}\right) + 0.157 \qquad (7)$$

Figure 1 is a plot of Equation (7) for the ranges of relative humidity, atmospheric pressure, and temperature expected in the marine atmospheric boundary layer. Notice that a well-mixed marine atmospheric boundary layer produces a modified refractivity gradient slightly greater than standard.

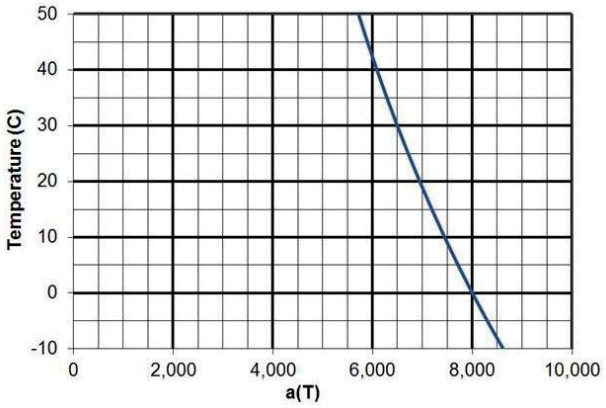

Figure 2. $a(t)$ **from Equation (8) at a pressure of** 10^3 **hPa.**

The mean of the 360 values of the vertical gradient of M in Figure 1 is $0.128\ \mathrm{m}^{-1}$. This allows for an instructive description of the vertical gradient of M more related to classic atmospheric-boundary-layer thermodynamic structure. Analysis of a wide range of global marine atmospheric-boundary-layer refractivity structures by the Naval Surface Warfare Center, Dahlgren Division, over the last ten years led to the observation that the vertical gradient of w is typically two to six times more influential on the vertical gradient of M than is the vertical gradient of θ. The radio-frequency engineer is highly knowledgeable about the influence of the dependent variable (M) in Equation (7) on RF system performance. The atmospheric-boundary-layer meteorologist is equally knowledgeable regarding the independent variables (θ, w) in Equation (8) and how they relate to classic marine atmospheric-boundary-layer thermodynamic structure. This equation has been successfully employed to exchange valuable knowledge between these two supporting disciplines. The blending technique presented in this paper occurs with $\theta(z)$ and $w(z)$ that leads to a calculation of $M(z)$.

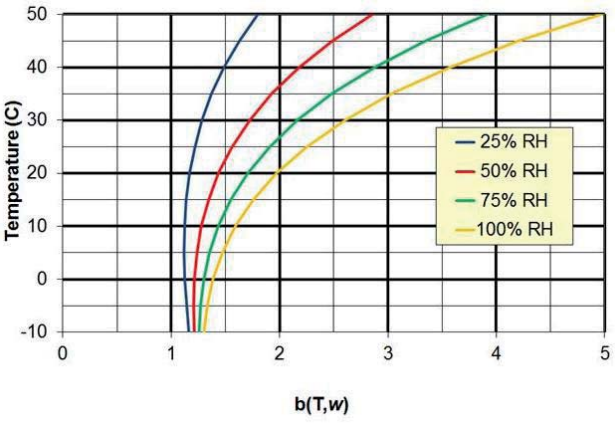

Figure 3. $b(T,w)$ **as a function of relative humidity (%RH) and temperature from Equation (8) at a pressure of** 10^3 **hPa.**

$$\frac{\partial M}{\partial z} \approx 0.128 + a(\theta)\frac{\partial w}{\partial z} - b(\theta, w)\frac{\partial \theta}{\partial z}. \qquad (8)$$

From Equation (6), it can be seen that $a(T)$ is weakly dependent on pressure and inversely proportional to the square of potential temperature. Figure 2 is a plot of $a(T)$ for a typical marine atmospheric boundary layer atmospheric pressure of 10^3 hPa for a range of expected temperatures in the marine atmospheric boundary layer. Figure 3 represents $b(T,w)$ over a range of relative humidity and temperature typical in the marine atmospheric boundary layer for an atmospheric pressure of 10^3 hPa.

In recent years, mesoscale numerical weather prediction (NWP) models have been investigated and employed for the purpose of providing prognostic location and time-specific refractivity fields [6-8]. Vertical profiles on horizontally spaced grids of the independent variables in Equation (1) support calculation of vertical profiles of M on the same structured grid. Vertical thermodynamic profiles are on discrete levels at each horizontal grid point. Due to roughness length and turbulence modeling requirements, these numerical weather prediction models can only provide data to within 5 m to 10 m of the sea's surface. With the atmosphere at the sea's surface near saturation, the rapid decrease in water vapor with height leads to refractivity structure with significant engineering impacts in this near-surface region, where numerical weather prediction models provide no thermodynamic profile data. Monin-Obukhov-Similarity (MOS) models have traditionally been employed to predict refractivity in the lowest layer, known as the atmospheric surface layer [9].

The complete vertical profile of M is thus created by blending two different types of models in a manner that does not produce non-physical gradients in M. The mesoscale numerical weather prediction model solves the prognostic equations based on Newton's second law of motion, the equations of state for an ideal gas, the first law of thermodynamics, conservation of mass, and conservation of moisture. The numerical weather prediction model predicts vertical profiles of wind speed, pressure, temperature, moisture, and modified refractivity at discrete vertical levels on a horizontal grid from the surface layer to the stratosphere, and produces vertical profiles every 1 km to 3 km every hour for a 48-hour forecast. The Monin-Obukhov Similarity model assumes that the atmospheric flow is horizontally homogeneous and quasi-stationary; that the turbulent fluxes of momentum, heat, and moisture are constant with height; that molecular exchanges are insignificant compared to turbulent exchanges; that rotational effects can be ignored; and that the influence of surface roughness, boundary-layer height, and geostrophic winds are fully accounted for by the ratio of the surface drag to the air density [10]. The Monin-Obukhov Similarity model parameterizes vertical thermodynamics leading to continuous profiles. For refractivity-profile predictions, the surface-layer model is

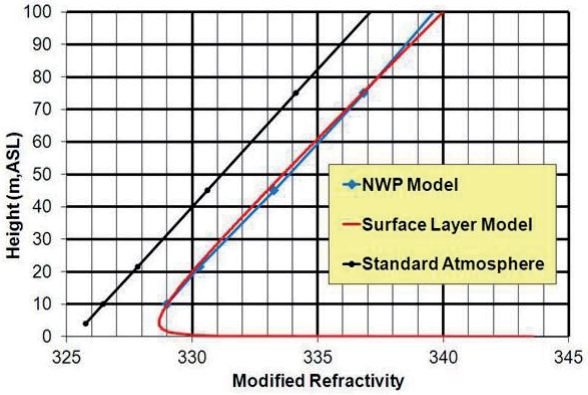

Figure 4. Modified refractivity examples represented by a Monin-Obukhov Similarity surface-layer model in red, and a numerical weather prediction model in blue. The marked data points for the blue numerical weather prediction model curve indicate vertical resolution. The black curve represents a standard atmosphere.

historically referred to as an evaporation-duct model. The problem is demonstrated in Figure 4.

The Monin-Obukhov Similarity surface-layer model in Figure 4 is driven by the wind speed, temperature, and water-vapor content predicted by the numerical weather prediction model at 10 m above sea level in the example in Figure 4. The remaining Monin-Obukhov Similarity surface-layer model input is the sea-surface temperature provided by the numerical weather prediction model at each numerical weather prediction model horizontal grid point. The dilemma, as posed in Figure 4, is to determine at what height to abandon the Monin-Obukhov Similarity surface-layer model and to transfer to the numerical weather prediction model. This must not only be accomplished without producing unrealistic vertical profiles of *M*, but it must be robustly performed for as many as 56,000 profiles associated with a 48-hour numerical weather prediction forecast.

2. A Zero-Order-Closure Turbulent Flux-Conservation Blending Technique

The use of numerical weather prediction modeling to predict RF system performance is becoming an internationally employed technology. As a result, multiple organizations have developed techniques for blending Monin-Obukhov Similarity and numerical weather prediction refractivity profiles. Prior to the use of numerical weather prediction models, blending techniques were designed for a more limited number of measured profiles of *M*, where an analyst in the loop was practical.

The Johns Hopkins University Applied Physics Laboratory, Direction general de l'armement (DGA, France), and the Naval Post Graduate School have developed blending techniques for modified refractivity profiles [11-13]. The Defence Science Technology Organisation determines the height of the surface layer in a refractivity-profile-assimilation model by assuming that the wind speed and friction velocity, as well as the potential temperature and temperature scale, are positively correlated at each analysis height [14]

The blending technique described in this paper differs from the techniques described above in two fundamental ways. First, the center of the blending layer is defined as the predicted height of the surface or constant-flux layer. Above this height, the validity of the surface-layer model becomes suspect. Secondly, the blending occurs in thermodynamic space (θ , w, and p), and the resulting blended M curve is calculated from the blended thermodynamic data. Our thinking is that since refractivity is a derived engineering variable, based on the thermodynamic vertical profiles found in natural atmospheric boundary-layer structures, blending is best accomplished at the thermodynamic level. Implicit in this thinking, compared to other models, is that we do not have to assume that ducting always occurs in the surface layer.

The height of the surface layer is defined by the height at which the turbulent fluxes vary by a mathematically tolerable level, commonly taken as 10% [15]. The height of the surface layer is determined by calculating the momentum, heat, and moisture flux at each numerical weather prediction model level, beginning at the lowest, using the Monin-Obukhov Similarity model output driven by the numerical weather prediction at that height. The Monin-Obukhov Similarity accepts sea-surface temperature, and temperature, humidity, and wind speed at each discrete numerical weather prediction height. It is assumed that the air at the surface is saturated, and the wind speed is zero. It is then determined at what increasing numerical weather prediction model height these turbulent fluxes first vary by more than 10% from the surface value, thereby testing one of the major assumptions of the Monin-Obukhov Similarity surface-layer model: that turbulent fluxes are constant with height [10]. Monin-Obukhov Similarity is a zero-order turbulence closure scheme where all resulting equations are fully parameterized [16]. Higher-order closure schemes that employ prognostic equations could be considered, but this Monin-Obukhov Similarity flux-profile approach appears to provide a suitable surface-layer height, leading to a robust engineering product. Two assumptions are made in this determination. It is assumed that the first numerical weather prediction model level is in the surface layer. It is also assumed that the fluxes vary linearly between discrete numerical weather prediction model levels.

The momentum flux is defined as the covariance of the turbulent components of the horizontal and vertical wind speeds:

$$\overline{uw} \equiv \text{vertical momentum flux} = u_*^2 , \qquad (9)$$

$u_* \equiv$ friction velocity $= Uk \Big/ \left[\ln\left(z/z_0\right) - \psi_m \right]$, (10)

where

$U \equiv$ mean wind speed at each NWP model height
$k \equiv$ von Karmon constant ≈ 0.4
$z \equiv$ height of each NWP model layer
$z_0 \equiv$ roughness depth
$\psi_m \equiv$ similarity function for momentum.

The heat flux is defined as the covariance of the turbulent components of potential temperature and vertical wind speed.

$$\overline{\theta w} \equiv \text{vertical heat flux } = \theta_* u_*, \quad (11)$$

$\theta_* \equiv$ turbulent heat scale

$$= \left(\Theta - \Theta_s\right) k \Big/ \left[\ln\left(z/z_0\right) - \psi_\theta \right], \quad (12)$$

where

$\Theta \equiv$ mean potential temperature at each NWP model height
$\Theta_s \equiv$ mean potential temperature at the surface
$\psi_\theta \equiv$ similarity function for heat
$\Theta = T\left(\dfrac{p_0}{p}\right)^{\dfrac{R}{c_p}}$
$p_0 = 10^3 hPa$
$p \equiv$ mean pressure at each NWP vertical level
$R \equiv$ gas constant for dray air 2.87×10^2 $\text{Jkg}^{-1}\text{K}^{-1}$
$C_p \equiv$ specific heat of dry air at constant pressure $= 1.00467 \times 10^3$ $\text{Jkg}^{-1}\text{K}^{-1}$.

The moisture flux is defined as the covariance of the turbulent components of specific humidity and vertical wind speed.

$$\overline{qw} \equiv \text{vertical moisture flux } = q_* u_*, \quad (13)$$

$q_* \equiv$ turbulent moisture scale

$$= \left(Q - Q_s\right) k \Big/ \left[\ln\left(z/z_0\right) - \psi_q \right], \quad (14)$$

where

$Q \equiv$ mean specific humidity at each NWP model height
$Q_s \equiv$ mean specific humidity at the surface
$\psi_q \equiv$ similarity function for humidity

$$Q = \frac{0.622e}{p - e} = \frac{w}{w + 1}$$

The similarity functions are empirical functions of the ratio of the height in the surface layer (z) to the Monin-Obukhov length (L). L is defined as the height in the surface layer where turbulent kinetic energy (TKE) produced by wind shear is equal to turbulent kinetic energy produced by buoyancy [10]. Using Equations (10), (12), and (14), the turbulent fluxes of momentum, heat, and moisture are calculated at each numerical weather prediction model vertical level, beginning at the lowest.

$$\overline{uw} = u_*^2 = \left\{ Uk \Big/ \left[\ln\left(z/z_0\right) - \psi_m \right] \right\}^2, \quad (15)$$

$$\overline{\theta w} = \theta_* u_* \left[\frac{\left(\Theta - \Theta_s\right) k}{\ln\left(z/z_0\right) - \psi_\theta} \right] \left[\frac{Uk}{\ln\left(z/z_0\right) - \psi_m} \right], \quad (16)$$

$$\overline{qw} = q_* u_* \left[\frac{\left(Q - Q_s\right) k}{\ln\left(z/z_0\right) - \psi_q} \right] \left[\frac{Uk}{\ln\left(z/z_0\right) - \psi_m} \right]. \quad (17)$$

The first height higher than the first numerical weather prediction model level that corresponds to a 10% change from the nearest surface value for any of the three fluxes is considered to be the point where the Monin-Obukhov Similarity surface-layer profile is gracefully abandoned for the numerical weather prediction profile. The surface-layer model employed in this work was the Navy Atmospheric Vertical Surface Layer Model (NAVSLaM) [17] version 1.0, and the numerical weather prediction model was the Coupled Ocean Atmosphere/Mesoscale Prediction System (COAMPS®) [18]. NAVSLaM was run at 0.25 m vertical resolution. COAMPS® was typically run with a 10 m vertical resolution in the surface layer and a 3 km horizontal resolution. The similarity functions used to calculate the turbulent fluxes at each numerical weather prediction height were those employed by NAVSLaM. L used to evaluate the similarity functions was also provided by NAVSLaM. Fluxes were calculated beginning at the lowest COAMPS® level, and progressing to subsequent higher levels until the fluxes departed from the lowest-level values by 10%.

The technique assumes the surface-layer height is the height at which the COAMPS® derived fluxes vary by 10% from the NAVSLaM (N) fluxes calculated for the constant-flux layer. As an example, examine moisture flux:

$$0.9 \geq \frac{q_C^* u_C^*}{q_N^* u_N^*} \geq 1.1,$$

q_C^* ≡ The required turbulent moisture scale at eachCOAMPS height to provide the specific humidity at that height

u_C^* ≡ The required turbulent momentum scale at each COAMPS height to provide the wind speed at that height

q_N^* ≡ The constant flux layer turbulent moisture scale calculated by NAVSLaM

u_N^* ≡ The constant flux-layer turbulent momentum scale calculated by NAVSLaM

$$q_N^* = \frac{\left(Q_{z,N} - Q_{0,N}\right)k}{\ln\left(\frac{z}{z_0}\right) - \Psi_q}$$

$$u_N^* = \frac{\left(U_{z,N} - U_0\right)k}{\ln\left(\frac{z}{z_0}\right) - \psi_m} = \frac{U_{z,N}k}{\ln\left(\frac{z}{z_0}\right) - \psi_m}$$

$$q_C^* = \frac{\left(Q_{z,C} - Q_{0,C}\right)k}{\ln\left(\frac{z}{z_0}\right) - \psi_q}$$

$$u_C^* = \frac{\left(U_{z,C} - U_0\right)k}{\ln\left(\frac{z}{z_0}\right) - \psi_m} = \frac{U_{z,C}k}{\ln\left(\frac{z}{z_0}\right) - \psi_m}$$

$$\frac{q_C^*}{q_N^*} = \frac{\left(Q_{z,C} - Q_{0,C}\right)}{\left(Q_{z,N} - Q_{0,N}\right)}$$

$$\frac{u_C^*}{u_N^*} = \frac{U_{z,C}}{U_{z,N}}$$

$$0.9 \geq \frac{q_C^* u_C^*}{q_N^* u_N^*} \geq 1.1$$

$$= 0.9 \geq \frac{\left(Q_{z,C} - Q_{0,C}\right)}{\left(Q_{z,N} - Q_{0,N}\right)} \frac{U_{z,C}}{U_{z,N}} \geq 1.1 \qquad (18)$$

Similarly, it can be shown for momentum flux and temperature flux, respectively,

$$0.9 \geq \frac{u_C^* u_C^*}{u_N^* u_N^*} \geq 1.1$$

$$= 0.9 \geq \left(\frac{U_{z,C}}{U_{z,N}}\right)^2 \geq 1.1 \qquad (19)$$

$$0.9 \geq \frac{\theta_C^* u_C^*}{\theta_N^* u_N^*} \geq 1.1$$

$$= 0.9 \geq \frac{\left(\Theta_{z,C} - \Theta_{0,C}\right)}{\left(\Theta_{z,N} - \Theta_{0,N}\right)} \frac{U_{z,C}}{U_{z,N}} \geq 1.1\,. \qquad (20)$$

It thus can be seen from Equations (18) to (20) that the determination of the surface-layer height is in fact calculated by the excursions of the COAMPS® bulk variables from the NAVSLaM bulk variables with height, and these do not depend on the form of the similarity functions.

2.1 Turbulent Flux Calculations

Example heat, momentum, and moisture turbulent flux calculations using Equations (15) to (17) and COAMPS® data are displayed in Figure 5 (COAMPS® is a registered trademark of the Naval Research Laboratory). The COAMPS® data points at 10 m, 22 m, 35 m, and 75 m are indicated. Because all of the required NAVSLaM input parameters were not available from COAMPS® at the surface, it was assumed that the lowest COAMPS® level was in the constant-flux layer, and the turbulent flux at that level was representative of the surface value. Flux values were assumed to vary linearly between discrete COAMPS® levels. The gold vertical bars were the ±10% excursion values. The heat flux varied by 10% from the lowest value at 14.8 m, the momentum flux varied by 10% at 18.2 m, and the moisture flux varied by 10% at 30.9 m. The height of the surface layer for this case was thus assumed to be 14.8 m, as predicted by the heat-flux profile. This height was then defined as the center of the blending zone.

2.2 Blending Zone

Analogous to molecular mean free path, Prandtl [19] proposed a turbulent mixing length over which a parcel of air will maintain identity before mixing with the surrounding fluid. In this blending technique, the Prandtl mixing length

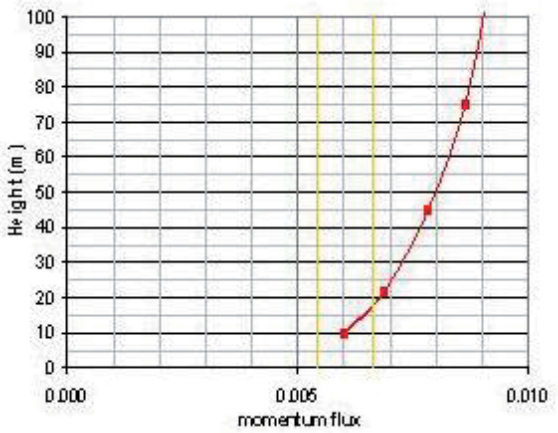

Figure 5a. The momentum flux in Nm^{-2}, calculated from the COAMPS® data depicted in Figure 4 and used in Equation (12). The gold vertical bars indicate the ±10% excursion from the nearest surface value.

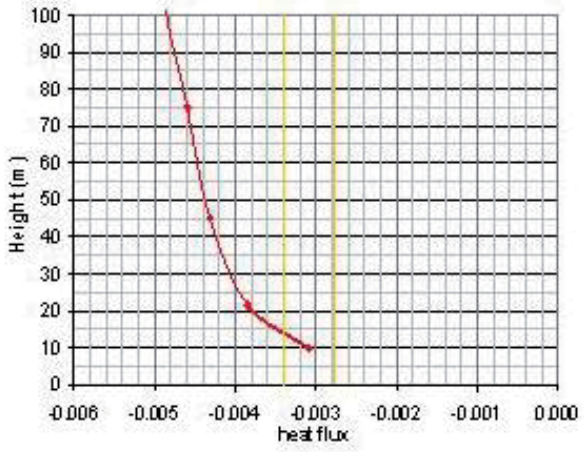

Figure 5b. The heat flux in Wm^{-2}, calculated from the COAMPS® data depicted in Figure 4 and used in Equation (13). The gold vertical bars indicate the ±10% excursion from the nearest surface value.

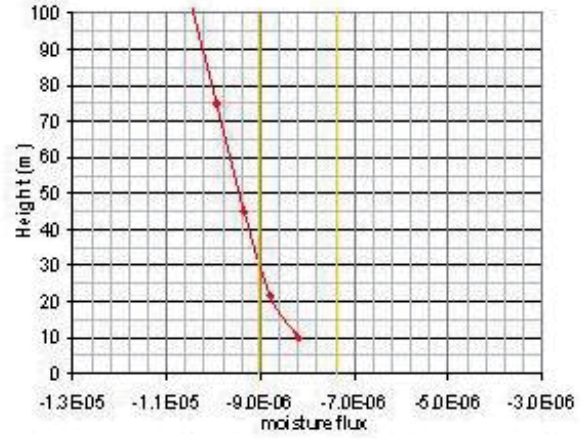

Figure 5c. The moisture flux in $kgsm^{-2}$, calculated from the COAMPS® data depicted in Figure 4 and used in Equation (14). The gold vertical bars indicate the ±10% excursion from the nearest surface value.

defines the depth of the blending zone, and is centered at the blending point determined by the flux-excursion method described in the previous section. There are many parameterizations available in the literature for the Prandtl mixing length. The formulation for the Prandtl mixing length chosen for this blending technique was developed by the European Centre for Medium Range Weather Forecasting (ECMWF) [20], and is displayed in Equation (21):

$$\frac{1}{l_m} = \frac{1}{k z_s} + \frac{1}{\lambda}, \qquad (21)$$

$l_m \equiv$ Prandtl mixing length
k = 0.4
$z_s \equiv$ surface-layer height
$\lambda = 150$ m.

For the surface-layer height of 14.8 m in this example, the resulting Prandtl mixing length from Equation (18) was 5.7 m. The resulting blending zone was from 11.9 m to 17.6 m. A $\ln^2(z)$ weighting function was employed every 0.25 m across the blending zone to create a smooth blend of the slopes of the NAVSLaM thermodynamic variables and the slopes of the COAMPS® thermodynamic variables. Linear interpolation was employed between discrete COAMPS® levels. The 0.25 m resolution was chosen as a conservative value for the purpose of resolving evaporation duct heights to within 1.0 m. A $\ln^2(z)$ function was chosen instead of a linear function to minimize the impact of the blend, and to allow the Monin-Obukhov Similarity and numerical weather prediction model data to provide the solution. The weighting function is shown for the current example in Figure 6.

The smoothed thermodynamic slope curves were

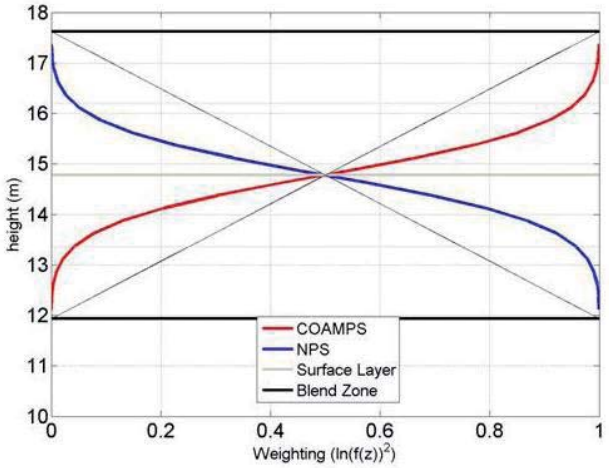

Figure 6. The weighting function for the numerical weather prediction and Monin-Obukhov Similarity models for a surface-layer height of 14.8 m and a blending length of 2.8 m.

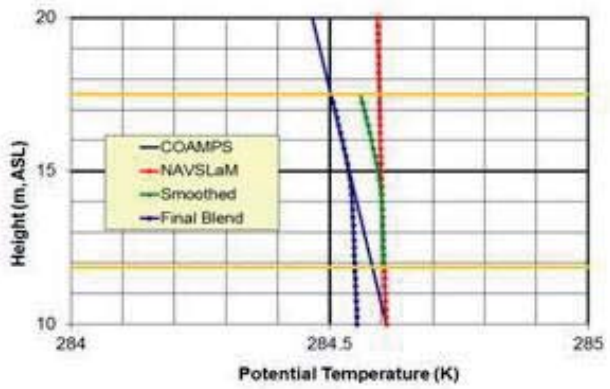

Figure 7a. The blending results for the potential temperature. The horizontal gold lines delineate the blending zone.

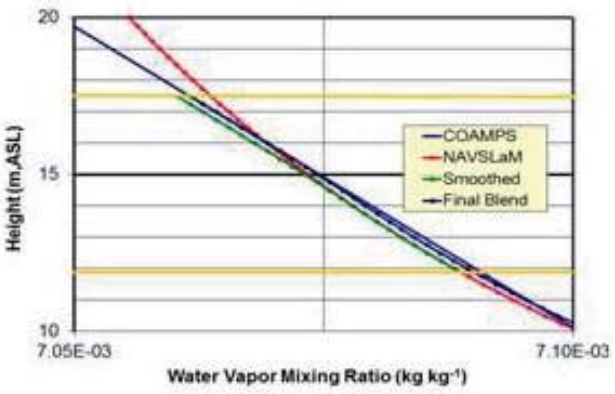

Figure 7b. The blending results for the water-vapor mixing ratio. The horizontal gold lines delineate the blending zone.

vertically integrated to produce vertical profiles of potential temperature and water-vapor mixing ratio. Because the Monin-Obukhov Similarity model and the numerical weather prediction model intercepted at the bulk parameter input level of 10 m, the blending of the thermodynamic curves had to be completed by sliding the blended curves toward the COAMPS® curves so that they matched at the top of the blending layer. This procedure did not affect the vertical gradient of refractivity or the resulting RF propagation. Atmospheric-pressure blending was accomplished in the same manner. This smoothing and blending technique for the current example is shown in Figure 7.

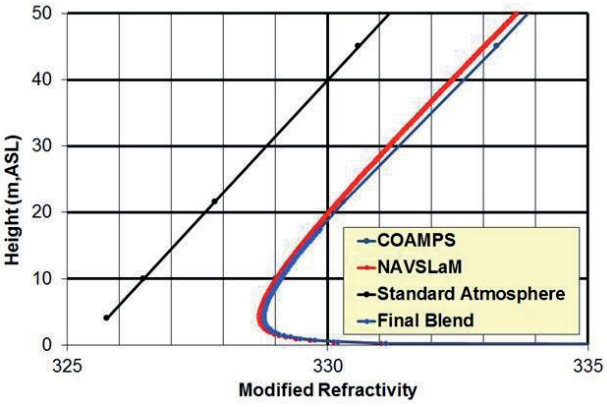

Figure 8. The final blending results for the modified refractivity.

The final blended values of θ and w were converted to T and e through Equations (3) and (4), respectively. The resulting final blended profile of M was calculated from Equation (2). The results for the current example are displayed in Figure 8.

2.3 Data Comparison

The Wallops 2000 Microwave Propagation Measurements Experiment [21] provided a multi-wavelength two-dimensional measured propagation data set for comparison with the blending technique described in the previous sections. Figure 9 delineates a 40 km path off Wallops Island, Virginia, USA where S-, C-, and X-band propagation measurements were made between 1512 UTC and 1605 UTC on April 28, 2000. The multi-wavelength propagation measurements were made from 0 m to 10 m above sea level along this 40 km path. A 3-km-horizontal-resolution COAMPS® grid for 1600 UTC was included the 40 km path. The COAMPS® data were processed by a Barnes objective analysis scheme [22, 23] to produce a meteorological profile along the bearing every 2 km. The blending technique described in the previous sections was applied to each of these 21 profiles. The location of the Naval Postgraduate School meteorological flux buoy is also indicated in Figure 9 [21]. Bulk meteorological parameters from this instrument were used to calculate a single surface-layer refractivity curve to be used with each

Figure 9. The propagation measurement bearing off Wallops Island, Virginia, USA, between 1512 UTC and 1605 UTC on April 28, 2000. The NPS flux meteorological buoy was located along the bearing approximately 13 km offshore.

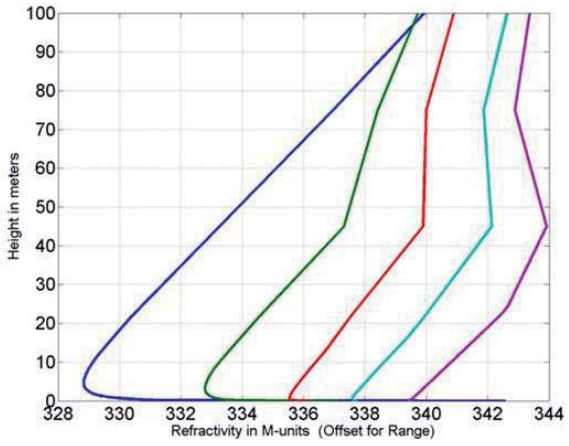

Figure 10. Blended modified refractivity profiles at 0 km, 10 km, 20 km, 30 km, and 40km along the bearing in Figure 9.

helicopter sounding collected along the 40 km path [21].

Figure 10 displays the thinned (for clarity) resulting range-dependent modified refractivity profiles at 0 km, 10 km, 20 km, 30 km, and 40 km, respectively from left to right along the path in Figure 9. The profile at 0 km was that described in the development of the blending technique in the previous sections. Notice the decrease in evaporation duct height in the offshore direction.

Comparisons of the measured S-band one-way propagation factor from 1512 UTC to 1605 UTC with the COAMPS®/NAVSLaM blend one-way propagation-factor prediction are provided in Figure 11. Propagation measurements were made from 0 m to 10 m above sea level along the 40 km path using the Microwave Propagation Measurement System (MPMS) [21]. The propagation modeling was performed by employing the 21 blended profiles along the bearing in Figure 9 with the tropospheric electromagnetic parabolic equation routine (TEMPER) [24]. TEMPER is a parabolic-wave-equation RF propagation model developed at the Johns Hopkins University-Applied Physics Laboratory that considers sea surfaces as well as terrain. At this wavelength, the first multipath null was not observed in this 10-m-deep layer. The difference graphic represents measurement minus model.

A similar analysis for the C-band measurements between 1512 UTC and 1605 UTC on April 28, 2000, is demonstrated in Figure 12. Notice that at this shorter wavelength, the first multipath null is observable in the top left corner. The X-band analysis is provided in Figure 13. Due to the even shorter wavelength, the multipath nulls were more prominent in this 10 m deep layer of one-way

Table 1. S-band comparison statistics.

	Refractivity Source	50th Percentile Absolute Error (dB)	90th Percentile Absolute Error (dB)
All Dates and Times	COAMPS®	0.8	2.4
All Dates and Times	Helicopter	1.3	3.4

Table 2. C-band Comparison Statistics.

	Refractivity Source	50th Percentile Absolute Error (dB)	90th Percentile Absolute Error (dB)
All Dates and Times	COAMPS®	1.2	3.1
All Dates and Times	Helicopter	1.8	4.7

Table 3. X-band Comparison Statistics.

	Refractivity Source	50th Percentile Absolute Error (dB)	90th Percentile Absolute Error (dB)
All Dates and Times	COAMPS®	1.2	5.3
All Dates and Times	Helicopter	2.2	6.8

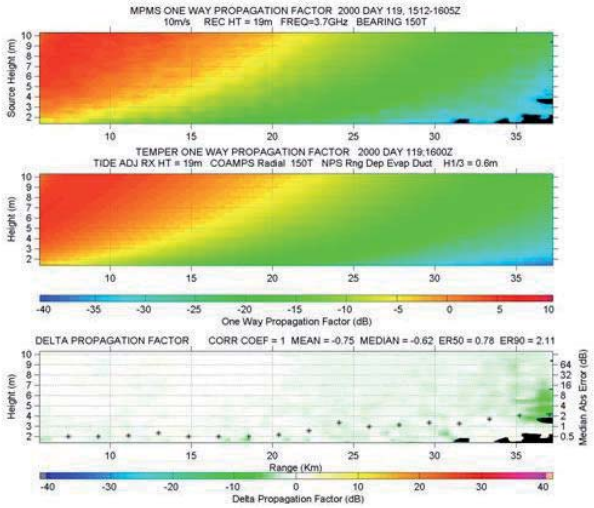

Figure 11. The S-band (3.7 GHz) propagation-factor measurements (upper graphic), the COAMPS®/NPS blend propagation-factor predictions (middle graphic), and the differences (lower graphic), plotted in range and height. The 50th percentile error was 0.8 dB, and the 90th percentile error was 2.1 dB.

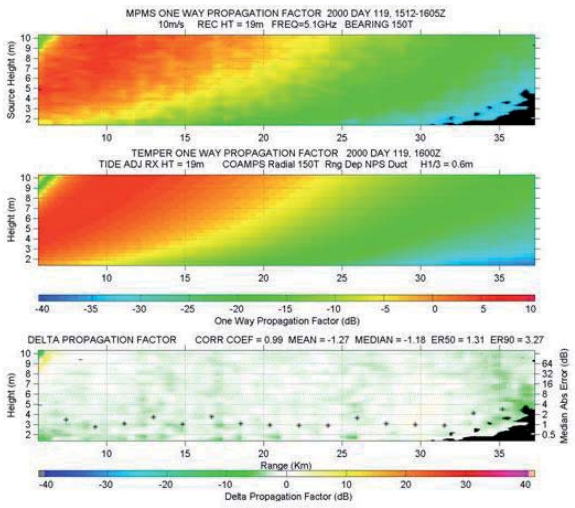

Figure 12. The C-band (5.1 GHz) propagation-factor measurements (upper graphic), the COAMPS®/NPS blend propagation-factor predictions (middle graphic), and the differences (lower graphic), plotted in range and height. The 50th percentile error was 1.3 dB, and the 90th percentile error was 3.3 dB.

propagation factor.

It is important to note that the measurement data was taken over nearly an hour as the transmitter boat sailed along the path in Figure 9. The marine atmospheric boundary layer and the resulting refractivity field were constantly slightly adjusting to the temperature and water vapor in the air flowing over the sea's surface during this period. This data comparison assumed that the propagation factor measured remained constant over this range during the period of collection. It could also be seen that as the multipath nulls showed in the close-range X-band data, the mean absolute error was increased.

A total of six two-dimensional propagation measurements made over three days were used for comparison with similar results. Tables 1 to 3 summarize the 50th and 90th percentile error results for the S, C, and X bands, respectively. They include not only the performance statistics for the COAMPS®/NPS blend, but also the performance statistics for predictions based on range-dependent meteorological soundings made by the Johns Hopkins University Applied Physics Laboratory helicopter [21]. In the case of a COAMPS®/NAVSLaM blend, it is a single COAMPS® model forecast hour. In the case of the helicopter, it is the period over which the meteorological helicopter sampled the vertical structure of the marine atmospheric boundary layer along the MPMS measurement bearing. In some cases, there were multiple helicopter runs for one MPMS propagation measurement. As is standard test and evaluation practice, the fully blended helicopter soundings were composed of helicopter measurements and a surface-layer model. NAVSLaM was driven by bulk inputs from the NPS buoy located approximately 13 km offshore, as in Figure 9. The blending technique was similar to those in the Multi-source Assimilation and Refractivity Interpolator (MARI) [11]. The same evaporation duct defined by data from the NPS buoy was blended with each range-dependent helicopter sounding.

It could be observed from Figures 11 to 13 and Tables 1 to 3 that the blending technique described in this paper produced relatively lower errors compared to measurements. In the median, over all the data-comparison events, the range-dependent COAMPS®/NAVSLaM blend surface-layer refractivity profiles produced slightly better

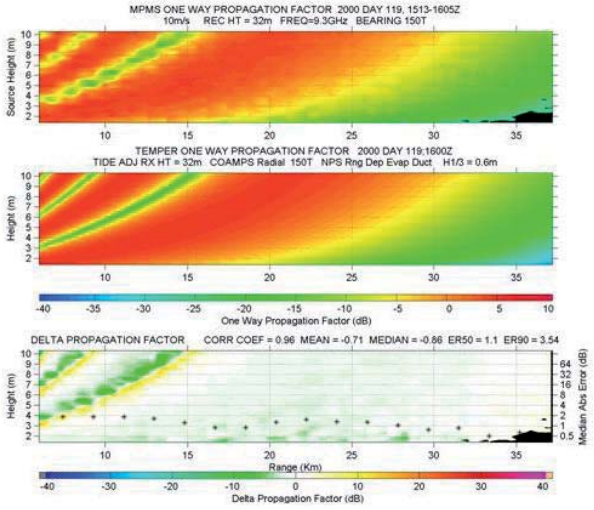

Figure 13. The X-band (9.3 GHz) propagation-factor measurements (upper graphic), the COAMPS®/NPS blend propagation-factor predictions (middle graphic), and the differences (lower graphic), plotted in range and height. The 50th percentile error was 1.1 dB, and the 90th percentile error was 3.5 dB.

results than the constant-evaporation-duct height profiles produced by blending the same surface-layer profile with each helicopter profile. It can also be seen that the measured minus modeled errors tended to increase with decreasing wavelength as the multipath nulls became more prominent.

3. Conclusions

A zero-order-closure turbulent flux-conservation technique for blending refractivity profiles from Monin-Obukhov Similarity and numerical weather prediction models has been described and compared with six two-dimensional multi-wavelength data sets. The technique is unique in that it determines the approximate depth of the surface layer at each numerical weather prediction grid point, and thereby defines the legitimate vertical domain for the surface-layer model at each numerical weather prediction grid point. Blending is accomplished over one Prandtl mixing length with the conserved thermodynamic variables. The blended thermodynamic variable curves are then employed to calculate the final blended modified refractivity profile at each numerical weather prediction grid point. The multi-wavelength data-comparison results indicated that the range-dependent COAMPS®/NAVSLaM surface-layer refractivity profiles in the median over all comparison data showed slight improvement relative to constant evaporation duct heights blended with range-dependent measured soundings.

4. Acknowledgement

This work was supported by the Office of Naval Research, Code 322, under N0001410AF00002.

5. References

1. B. R. Bean and E. J. Dutton, *Radio Meteorology*, New York, Dover Publications, 1968, p. 435.

2. D. E. Kerr, *Propagation of Short Radio Waves*, London, UK, Peter Peregrinus Ltd., 1987, pp. 191-192.

3. H. A. Hsu, *Coastal Meteorology*, San Diego, CA, Academic Press, Inc., 1988, pp. 206-207.

4. J. M. Wallace and P. V. Hobbs, *Atmospheric Science: An Introductory Survey*, San Diego, CA, Academic Press, 1977, pp. 68-76.

5. R. B. Stull, *An Introduction to Boundary Layer Meteorology*, Dordrecht, The Netherlands, Kluwer Academic Publishers, 1988, pp. 10-11.

6. T. Haack, C. Wang, S. Garrett, A. Glazier, J. Mailhot and R. Marshall, "A Mesoscale Model Inter-Comparison of Boundary Layer Refractivity and Atmospheric Ducting," *Journal of Applied Meteorology and Climatology*, **49**, 12, December 2010, pp. 2437-2457.

7. C. Wang, D. Wilson, T Haack, P Clark, H. Lean, R. Marshall, "Effects of Initial and Boundary Conditions of Mesoscale Models on Atmospheric Refractivity," *Journal of Applied Meteorology and Climatology*, **51**, 1, January 2012, pp. 115-132.

8. R. E. Marshall, W. D. Thornton, G. H. Lefurjah and T. S. Casey, "Modeling and Simulation of Notional Future Radar in Non-Standard Propagation Environments Facilitated by Mesoscale Numerical Weather Prediction Modeling," *Naval Engineers Journal*, **120**, 4, December 2008, pp. 55-66.

9. J. C. Wyngaard, and O. R. Cote, "The Budgets of Turbulent Kinetic Energy and Temperature Variance in the Atmospheric Surface Layer," *Journal of the Atmospheric Sciences*, **28**, 2, March 1971, pp.190-201.

10. S. P. Arya, *Introduction to Micrometeorology*, San Diego, CA, Academic Press, 2001, pp. 213-223.

11. A. K. Kochhar, "Multiple-Source Assimilation and Refractivity Interpolator (MARI)," USNC/URSI National Radio Science Meeting, Albuquerque, NM, July 9-14, 2006.

12. J. Claverie, E. Mandine and Y. Hurtaud, "PREDEM: un nouvel outil de simulation pour la prédiction des performances des systèmes radars," ECPS Conference, Brest, France, March 15-18, 2005.

13. P. Frederickson, "An Evaluation of the Use of Mesoscale Numerical Weather Prediction Model Data with Electromagnetic Propagation Tactical Decision Aids," USNC/URSI National Radio Science Meeting, Boulder, CO, January 5-8, 2011.

14. D. M. Phillips and C. P. Baker, "Refractivity Profile Assimilation Model the Atmospheric Boundary Layer," Defence Science and Technology Organisation, Rep. DSTRO-RR-0148, Salisbury, South Australia, July 1999.

15. G. S. Poulos and S. P. Burns, "An Evaluation of Bulk Ri-Based Surface Layer Flux Formulas for Stable and Very Stable Conditions with Intermittent Turbulence," *Journal of the Atmospheric Sciences*, **60**, 20, October 15, 2003, pp. 2523-2537.

16. M. Z. Jacobson, *Fundamentals of Atmospheric Modeling*, Cambridge, UK, Cambridge University Press, 2005, p. 237.

17. P. A. Frederickson, K. L. Davidson, and A. K. Goroch, "Operational Bulk Evaporation Duct Model for MORIAH, Ver.1.2," Naval Postgraduate School, Rep. NPS/

MR-2000-002, Monterey, CA, 2000.
18. R. M. Hodur, X. Hong, J. D. Doyle, J. Pullen, J. Cummings, P. Martin, and M. A. Rennick, "The Coupled Ocean Atmosphere Prediction System (COAMPS)," *Oceanography*, **15**, 1, 2002, pp. 88-99.

19. L. Prandtl, "Bericht ueber Untersuchungen zur ausgebileten Turbulenz," *ZAMM*, **3**, 1925, pp 136-139.

20. P. White et al., "Part IV: Physical Processes," in *ECMWF IFS documentation CY25R1*, European Centre for Medium-Range Weather Forecasting, Reading, United Kingdom, 2003.

21. J. Stapleton, D. Shanklin, V. Wiss, T. Nguyen, and E. Burgess, "Radar Propagation Modeling Assessment Using Measured Refractivity and Directly Sensed Propagation Ground Truth," Naval Surface Warfare Center Dahlgren Division, Rep. NSWCDD/TR-01/132, Dahlgren, VA, 2001.

22. S. L. Barnes, "A Technique for Maximizing Details in Numerical Weather Map Analysis," *Journal of Applied Meteorology and Climatology*, **3**, 4, August 1964, pp. 396-409.

23. S. L. Barnes, "Mesoscale Objective Map Analysis Using Weighted Time-Series Observations," *Technical Memorandum ERL NSSL*, **62,** 1973, p. 60.

24. G. D. Dockery, R. S. Awadallah, D. E. Freund, J. Z. Gehman and M. H. Newkirk, "An Overview of Recent Advances for the TEMPER Radar Propagation Model," Proceedings of the IEEE Radar Conference, April 2007, pp. 896-905.

Introducing the Authors

Robert E. Marshall received a BS and MS in Electrical Engineering from Virginia Tech in 1971 and 1973, respectively. He taught radio-frequency engineering at Virginia Tech from 1973-1983 while investigating satellite-path attenuation and depolarization due to precipitation as a member of the Satellite Communications Group. He earned a PhD in Atmospheric Science from North Carolina State University in 1995, specializing in radar and atmospheric-boundary-layer meteorology. Dr. Marshall is a retired senior scientist at the Naval Surface Warfare Center in Dahlgren, Virginia, where he performed research in RF propagation and numerical weather prediction. He is currently the US National Committee for the International Union of Radio Science representative to the American Meteorological Society.

Victor R. Wiss received his BS in Electrical Engineering with emphasis in Physical Phenomena from Tennessee Technological University in 1984. He has worked in the research, development, testing, and evaluation of radar systems for the Naval Surface Warfare Center, Dahlgren Division, for 25 years. For the last 15 years, he has served as Lead Engineer for radio-frequency propagation and meteorological measurements.

Katherine L. Horgan received a BS in Meteorology from North Carolina State University in 2006. She is currently working on her MS in Atmospheric Science from Texas Tech University. Katherine is a scientist at the Naval Surface Warfare Center in Dahlgren, Virginia, where she performs research in meteorology and RF propagation.

William D. Thornton received a BS in Chemistry from Athens College, AL, in 1974. Mr. Thornton worked with AAW Fire Control Radar Systems for 30 years at Naval Surface Warfare Center in Dahlgren, VA. For the past 12 years he has worked in the fields of estimating radar-propagation performance in littoral clutter environments.

Janet K. Stapleton graduated with honors from Tennessee Technological University in 1985 with a bachelor's degree in Electrical Engineering. Upon graduation, she joined the Naval Surface Warfare Center in Dahlgren, VA. Throughout her career, she has supported a variety of Navy research and development programs. Many of these endeavors were related to low-altitude propagation of radio-frequency (RF) signals. The culmination of Mrs. Stapleton's work in RF propagation came with the Office of Naval Research project responsible for the measured data used in this report, where Mrs. Stapleton served as the Principal Investigator. Mrs. Stapleton is currently on staff in the Radar Development Branch of the Electromagnetic and Sensors Systems Department at the Naval Surface Warfare Center, Dahlgren Division. Mrs. Stapleton has been a member of USNC/URSI Commission F on Wave Propagation and Remote Sensing since 1996.